Dislocations mediate hydrogen retention in tungsten

2014 Nucl. Fusion 54 042004

(http://iopscience.iop.org/0029-5515/54/4/042004)

IOP Publishing | International Atomic Energy Agency Nuclear Fusion
Nucl. Fusion **54** (2014) 042004 (5pp) doi:10.1088/0029-5515/54/4/042004

Letter

Dislocations mediate hydrogen retention in tungsten

D. Terentyev[1], V. Dubinko[2], A. Bakaev[1,3], Y. Zayachuk[1], W. Van Renterghem[1] and P. Grigorev[1,4]

[1] SCK·CEN, Nuclear Materials Science Institute, Boeretang 200, Mol, 2400, Belgium
[2] National Science Center, Kharkov Institute of Physics and Technnology, Kharkov 61108, Ukraine
[3] Center for Molecular Modeling, Department of Physics and Astronomy, Ghent University, Technologiepark 903, 9052 Zwijnaarde, Belgium
[4] Department of Applied Physics, Ghent University, St. Pietersnieuwstraat 41, 9000 Ghent, Belgium

Received 12 November 2013, revised 9 January 2014
Accepted for publication 26 February 2014
Published 21 March 2014

Abstract

In this letter, a comprehensive mechanism for the nucleation and growth of bubbles on dislocations under plasma exposure of tungsten is proposed. The mechanism reconciles long-standing experimental observations of hydrogen isotopes retention, essentially defined by material microstructure, and so far not fully explained. Hence, this work provides an important link to unify material's modelling with experimental assessment of W and W-based alloys as candidates for plasma facing components.

Keywords: dislocations, tungsten, retention, hydrogen

S Online supplementary data available from stacks.iop.org/NF/54/042004/mmedia

(Some figures may appear in colour only in the online journal)

Development of fusion technology for electrical power production is one of the biggest challenges faced in 21th century. Its realization must overcome a number of challenges, one of which is the selection of appropriate plasma facing materials (PFM). *High flux* plasma exposure degrades properties of materials and leads to permeation and trapping of plasma components including highly toxic tritium (phenomenon known as *retention*). Low erosion/sputtering, high melting point and controlled retention are typical prerequisites of PFM, among which *tungsten* (W) is the main candidate [1, 2].

The retention of hydrogen (H) isotopes is attributed to their trapping at lattice defects resulting in the formation of bubbles and their subsequent growth into sub-surfaces blisters. The conventional analysis of the retention under high energy ion implantation is based on the premise that vacancies, generated in collision cascades, are responsible for the nucleation of stable H-vacancy clusters [3–5]. In International Thermonuclear Experimental Reactor (ITER), the energy of impinging ions (<100 eV) is well below the displacement threshold, and the implantation range is limited to several nanometers. Nevertheless, samples exposed at linear plasma generators, demonstrate that the H permeation extends up to several micrometers (μm) [6, 7]. At such depths, deep permeation of H cannot be assigned to the vacancy trapping as their equilibrium concentration is negligible at typical temperatures accessible to existing plasma generators, i.e. 300–800 K.

Grain boundaries were suggested as nucleation sites for bubbles [8], however, the retention also takes place in the recrystallized W [9] and even in single crystal W [10]. The self-trapping and nucleation of stable H clusters in W bulk is ruled out as a pair and triplet of H atoms exhibit negligible binding energy (~0.01 eV [11]). Moreover, different impurity concentrations do not result in any significant difference in the H depth profiles. Hence, the mechanisms of H retention provoking intensive blistering and bubble formation under sub-threshold plasma exposure are still to be identified.

In this letter, we explore the interaction of H with screw dislocations (SDs), the main microstructural features of metals including W. Using density functional theory (DFT) calculations, we demonstrate that H atoms are strongly bound to the SD core and exhibit fast one-dimensional (1D) migration along the dislocation line. An elementary dislocation segment accepts up to six H atoms practically without losing the interaction strength. Once the cluster of eight H atoms

is formed, it spontaneously transforms into an immobile configuration by punching out a jog on a dislocation line. The DFT data are incorporated in continuum rate theory model to evaluate the nucleation rate of H bubbles on a dislocation network as a function of depth. A good agreement with the experimental profiles suggests that dislocation microstructure is primarily responsible for the trapping of H isotopes under high flux plasma exposure. The TEM analysis performed on the W samples, exposed to plasma in our previous work [12] in conditions not yet featuring the blisters, reveals the presence of numerous nanometric cavities decorating dislocations with a linear density matching the predictions of our calculations.

To assess H–SD interaction we used the Vienna Ab-Initio Simulation Package (VASP) [13]. The projected augmentation wave [14] and the generalized gradient approximation [15] were used for the pseudopotential and the exchange-correlation potential, respectively. The 1s state for H and 5d6s states for W are treated as valence states. The atomic relaxation is carried out using the conjugate-gradient algorithm with the force convergence criterion of 0.03 eV Å^{-1}. The migration energy barrier is calculated using the nudged elastic-band (NEB) method with the quick-min algorithm [16], considering seven intermediate images with the same force convergence criterion of 0.03 eV Å^{-1}.

The dislocation dipole approach [17] is applied to model a $1/2\langle 1\,1\,1\rangle$ SD in a periodic crystal. Two SDs with antiparallel Burgers vectors are inserted into an ideal bcc W crystal, forming a dislocation quadruple [18]. A principal unit cell consists of three non-equivalent (1 1 1) atomic layers and has dimensions of $41.01 \times 38.82 \times 2.75$ Å^3 in the $[\bar{1}\,\bar{1}\,2]$ (x), $[1\,\bar{1}\,0]$ (y) and [1 1 1] (z) directions, which amounts to 135 W atoms in total. It is known to provide a reliable core structure and dislocation self-interaction brings negligible effect on the core properties [19]. This and twice larger (replicated in the [1 1 1] direction) unit cells are used in this work. More details on VASP parametrization are provided in the online supplementary material (stacks.iop.org/NF/54/042004/mmedia).

Firstly, the site preference for an interstitial H near the SD core was determined. The H–SD binding energy for all tetra- and octahedral interstitial sites (henceforth TIS and OIS) was computed as $E^{\mathrm{b}}_{\mathrm{H-SD}} = (E_{\mathrm{H+SD}} + E_{\mathrm{Bulk}}) - (E_{\mathrm{SD}} + E_{\mathrm{H}})$. $E_{\mathrm{H+SD}}$, E_{SD}, E_{H} are the total energy of the crystals containing, respectively, H and SD dipole simultaneously, only the SD dipole or H atom. E_{Bulk} is the total energy of the perfect W crystal with the same dimensions as used to model the SD dipole. Negative $E^{\mathrm{b}}_{\mathrm{H-SD}}$ implies that a system gains energy due to association of objects. Therefore, attractive interaction between two objects will correspond to the negative binding energy. The resulting 2D map zoomed near the SD core is given in figure 1(a). The SD core is composed of three $\langle 1\,1\,1\rangle$ atomic rows connected by the dashed black arrows in figure 1(a) (as it is conventionally represented by differential displacement analysis [20]). H atoms placed in OISs far from the core are unstable and relax to TISs. Few metastable OIS near the core are defined, but still occupation of TIS is more favorable. This corresponds to the fact that in W bulk, H also prefers to occupy TIS rather than OIS, with the energy difference of ~0.4 eV [21].

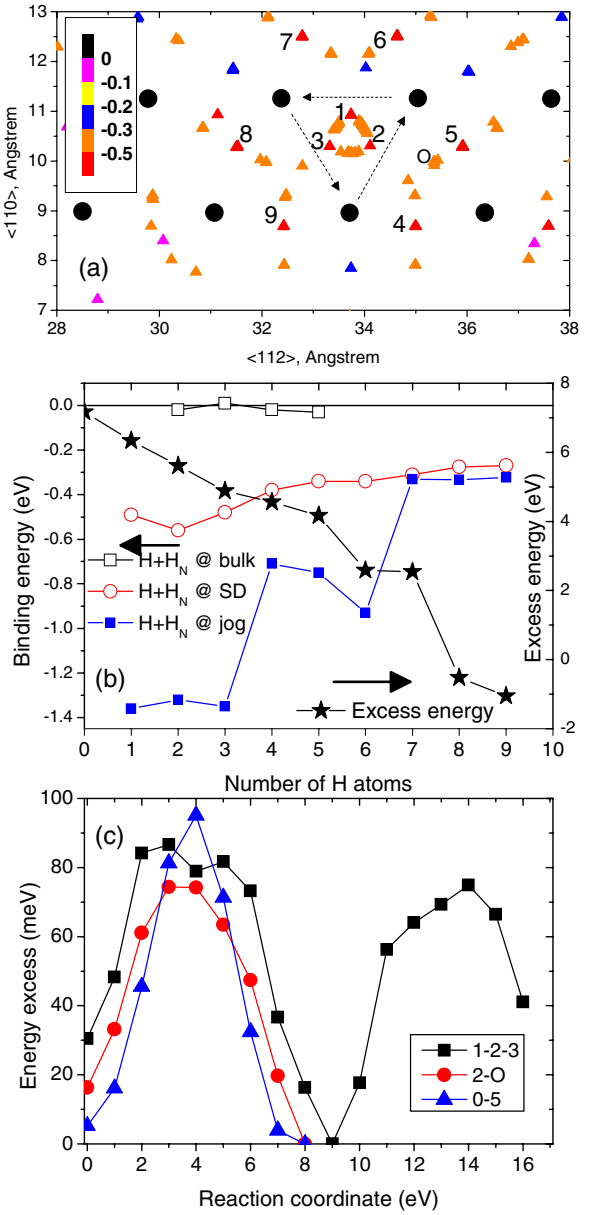

Figure 1. (a) H–SD binding energy map. Color code denotes the binding energy value in eV, note that H exhibits negative binding energy (i.e. attracted) in all positions near the dislocation core. Filled triangles display all metastable H positions, black circles display W atoms. Three dashed arrows show the $\langle 1\,1\,1\rangle$ atomic rows forming the SD core. (b) Left axis—incremental binding energy of H to H_N cluster placed in W bulk, or on the perfect dislocation core, or on the jogged dislocation core. Right axis—the excess energy as a function of H_N size to punch out the jog. (c) Migration energy paths between the metastable positions indicated in (a).

The binding energy map reveals three deep (equivalent) energy minima states for H atom inside the core and six especially favorable (and again equivalent) positions adjacent to the core, enumerated from 1 to 9 in figure 1(a). These positions coincide with TISs, where H atom is bound to the core with the energy of ~0.55 eV. Analysis of the charge distribution reveals that these positions coincide with the regions depleted by charge density (see the online supplementary material figure S.1(a)(stacks.iop.org/NF/54/042004/mmedia)), also interrelated with the distribution of local stress around the core.

The strong binding therefore originates from the compensation of local charge density (see the online supplementary figure S.1(*b*)(stacks.iop.org/NF/54/042004/mmedia)). Adding the second and the third H reduces the depleted region (see the online supplementary figures S.1(*c*) and (*d*)(stacks.iop.org/NF/54/042004/mmedia)) but does not cover it completely, pointing at a possibility of multiple trapping.

We therefore explored the binding energy and site preference for multiple H_N clusters adding them on a SD line in the nine revealed local minima i.e. forming a (1 1 1) platelet (henceforth H_N–SD cluster). For each relaxed H_N–SD configuration we computed the incremental binding energy for an extra H atom, presented in figure 1(*b*). A progressive removal of the depleted zone begins once $N > 3$. Addition of the fourth H atom results in a decrease of the absolute value of the binding energy. The most energetically favorable sequence to add H atoms is shown by numbers in figure 1(*a*). Starting from the seventh H atom, it is more favourble to continue growing the cluster along the dislocation line (i.e. place H in the next in-core position) rather than to build a (1 1 1) platelet. After adding the 8th H atom, we observed a considerable reconstruction of the H_N–SD cluster accompanied by a shift of W atoms forming the SD core. We attribute this to the formation of a pair of jogs, namely: a vacancy jog occupied by H_N cluster and an interstitial jog pushed aside. This process is analogous to the interstitial punching mechanism in the case of He self-trapping in bulk Fe [22].

To validate this hypothesis, we have computed the energy balance $E_{EX} = [E(H_N - SD) + E(SD)] - [E(H_N - JOG_V) + E(JOG_I)]$. Here, $E(SD)$ and $E(H_N–SD)$ are the total energies of the crystals containing, respectively, SD dipole and H_N cluster attached to SD core, while, $E(H_N–JOG_V)$ and $E(JOG_I)$ are the energy of crystals with H_N cluster attached to a vacancy jog and SD dipole containing an interstitial jog. A positive value of E_{EX} implies that the jog-punching is not favorable, while a negative value points to an exothermic reaction expected to occur spontaneously.

The vacancy and interstitial jogs were constructed, respectively, by removing and adding one W atom from/to the core of the SD. The formation energies for JOG_I and JOG_V were computed to be 7.2 eV and 2.23 eV, respectively. Their sum is by 3.8 eV lower than the Frenkel pair formation energy in W bulk, which is 9.73 + 3.5 eV being the formation energy for a vacancy and a self-interstitial atom, computed here in a 128 atomic supercell. As the creation of a pair of anti-jogs costs less energy than the Frenkel pair formation, a threshold for jog-punching on SD core may occur for a relatively low N still affordable for DFT techniques. E_{EX} as a function of N is shown in figure 1(*b*), which proves that the spontaneous jog-punching occurs once $N \geqslant 8$. In addition, we have calculated the binding energy of H to a H_N cluster on a vacancy jog. Note that the trapping of H at a pre-existing jog is much stronger, practically comparable to the binding energy for a single vacancy [5]. Therefore, jogs on dislocation lines, formed due to e.g. cyclic deformation under transient heat loads, will act as additional trapping sites for hydrogen and its isotopes.

Finally, we explored a possibility for H atom trapped on the SD core to exhibit 1 D migration that is viewed as a mechanism by which H_N clusters may grow and reach the

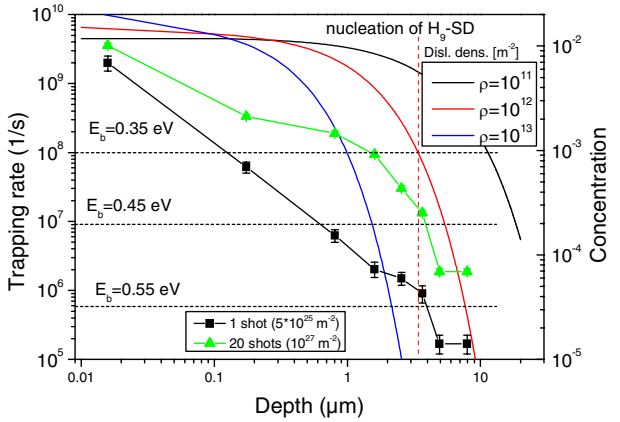

Figure 2. Left Y axis presents the reaction rates for H trapping by stable H_N-SD clusters versus depth calculated using equations (2*a*) and (2*b*)–(3) at 460 K, varying dislocation density in the range 10^{11}–10^{13} (m^{-2}). Horizontal black dashed lines reveal dissociation rates, $\bar{w}_n$, of H from H_N–SD clusters with $N = 1$–3 ($E_b = 0.55$ eV), $N = 4$–6 ($E_b = 0.45$ eV), $N = 7$–9 ($E_b = 0.35$ eV) obtained using equation (3). A vertical red dashed line specifies the depth threshold until which the nucleation of supercritical H_9–SD clusters takes place given the dislocation density and exposure temperature. Right Y axis displays the concentration of H isotope, deuterium, as a function of depth measured using nuclear reaction analysis techniques applied to the samples exposed to high flux plasma at 460 K as described in [23, 27]. The total fluence corresponding to the two exposures is given in figure on the inset.

critical size. Considering the site preference near the SD core, shown figure 1(*a*), we have explored two migration trajectories, namely: 'in-core' and 'out-core' paths. The former migration mode involves jumps between positions 1–2–3. The migration from the inner (shown by three arrows in figure 1(*a*)) to outer part of the core requires a jump from '2' to 'O' (octahedral site) and from 'O' to'5'. By performing a sequence of 'O–5–O' jumps H atom may migrate along the dislocation line being adjacent to its core. The computed excess energy profiles are provided in figure 1(*c*). In all the cases, the migration barrier does not exceed 0.1 eV, proving a possibility for fast 1D migration of H along the SD line at room temperature and above. In addition, H is fully flexible to occupy any of the nine trapping TISs (see figure 1(*a*)), as the transition barriers are also extremely low.

The above presented DFTC results are applied to treat a series of recent experiments on H retention in W exposed to high flux plasma (see our previous work [23]). We used the kinetic rate theory method and couple 3D bulk and 1D dislocation diffusion modes (see e.g. [24, 25]). The duration of the plasma impulse was 70 s and the surface temperature was 460 K. A typical retention profile obtained by nuclear reaction analysis (NRA) in such experiments shows that the H concentration drops sharply after several μm (see right hand-side Y-axis in figure 2).

A free path of the H along a dislocation before its detrapping to the bulk is given by [24]

$$\lambda_d^0 = b \exp\left(\frac{E_m^b - E_m^d + E_b^1}{2k_B T}\right) \quad (1)$$

where $E_b^1 = -E_{H-SD}^b$ i.e. the absolute value of the H–SD binding energy, E_m^d and E_m^b is, respectively, the migration

energy of H along SD core and the migration energy in the bulk ($E_m^b = 0.4$ eV [26]); b is the dislocation Burgers vector ~2.8 A. At 460 K, λ_d^0 exceeds 10 μm implying that trapped H atoms practically do not dissociate from the dislocation core prior to reaching a grain boundary interface or a free surface. While migrating along the core, H atoms will form H_N–SD clusters.

The rate of the formation of H_N–SD clusters on a dislocation segment of length λ_d located at a depth x, hereafter called $w_n^+(x)$ [s^{-1}], is given by the product of the H flux from bulk to the dislocation unit length, J_H^d [particles m^{-1} s^{-1}], and λ_d:

$$w_n^+ = J_H^d \lambda_d, \tag{2a}$$

$$J_H^d = \frac{Z_d}{w} D_H^b C_H^b(x) \tag{2b}$$

where Z_d ~1 is the dimensionless dislocation capture efficiency for H atoms diffusing from the bulk [25] with the diffusion coefficient, D_H^b, and ω is the atomic volume ~15 A^3. λ_d therefore becomes the mean spacing of H_N–SD clusters forming on dislocation lines. $w_n^+(x)$ depends on the depth via the bulk H concentration, $C_H^b(x)$, given by a steady-state solution of the diffusion problem of H in the effective medium with homogeneously distributed sinks:

$$C_H^b(x) = \frac{\omega F_H x_H}{D_H^b} \exp(-x k_H), \quad k_H \approx (Z_d \rho_d)^{0.5} \tag{3}$$

where F_H is the H flux, x_H is the implantation straggling (~1 nm), and k_H (m^{-1}) is a measure of the sink strength for migrating H atoms to be absorbed by dislocations with density, ρ_d [m^{-2}]. Equation (3) is valid at a steady-state condition (i.e. for times longer than it takes for H to reach a depth x). Given the duration of plasma exposure (70 s), H migration energy (0.4 eV) and sample temperature (460 K), a steady-state profile of equation (3) is established at a longer time than H diffusion through the region of interest takes (i.e. H covers 10 μm per second). The depth of H penetration and the corresponding H clustering rate are therefore essentially determined by the dislocation density, as shown in figure 2.

The balance of trapping (equations 2(a)–(b)) and detrapping of H atoms to/from H_N–SD clusters will define the condition for the formation of critical H_8–SD clusters and the condition for the jog-punching. The detrapping rate, w_n^-, is independent of depth and is defined as

$$w_n^- = w_0 \exp\left(-\frac{E_b^n + E_m^d}{k_B T}\right) \tag{4}$$

where E_b^n is the incremental binding energy of H to H_N−SD cluster given in figure 1(*b*) and ω_0 is the attempt frequency factor (taken as 10^{13} s^{-1}) The rates, w_n^-, obtained for the relevant exposure conditions [23] are plotted in figure 2. For the medium dislocation density (i.e. typical for annealed BCC metals) H permeation extends to a several μm thick layer, in which $w_n^+(x) > w_n^-$ and therefore the supercritical clusters are expected to form there, which is in a good agreement with the NRA profiles, also shown in figure 2.

As the clustering process starts, the actual linear number density of H_N–SD clusters (N_C [m^{-1}]) will define λ_d as soon as N_C will exceed $\rho_d \cdot \lambda_d^0$. Accordingly, the trapping rate will decrease inversely proportional to N_C, which will limit the number density of H_N–SD clusters. Applying the DFT data on H_N-SD binding, we estimated $N_C^{max} \approx 10^{19}$–$10^{20}$ m^{-3}, corresponding to the mean cluster spacing $\lambda_d \approx$ 100–10 nm.

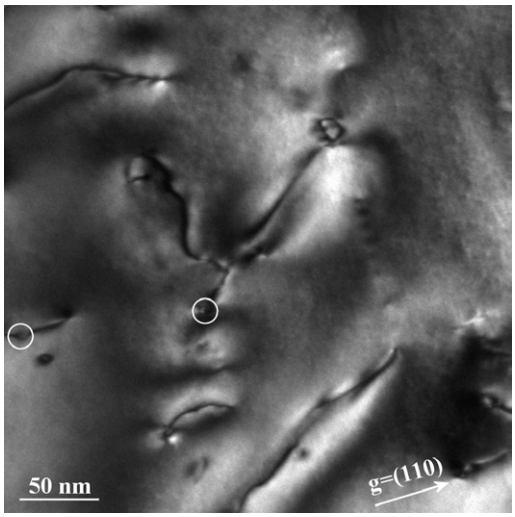

Figure 3. Dark field TEM image of screw dislocations decorated by H clusters. Two examples are indicated by the white circles.

Following the analytical assessment, the samples exposed in the above discussed experiment (i.e. with pre-defined depth profiles) have been inspected by transmission electron microscopy (TEM). To retain the plasma-induced damage, the samples were polished from the opposite site of the plasma exposure only. As an example, a typical dark field image showing SD lines decorated by cavities is given in figure 3. The dislocation density was roughly estimated to be in the range of 10^{12}–10^{13} m^{-2}, i.e. above the 'medium' value as expected since the exposed samples were double forged. The amount of visible hydrogen clusters is rather low for an accurate statistical determination, but based on the inspection of dozens of images, a mean linear spacing of 100 ± 20 nm was obtained, which is in the range estimated using the rate theory analysis.

We have therefore proposed and defended a comprehensive mechanism for the nucleation and growth of hydrogen bubbles on dislocation lines under high flux plasma exposure of tungsten. The mechanism comprises the following stages: interstitial H atom trapping at dislocation lines, its fast 1D migration, growth of multiple H_N clusters eventually resulting in the punching of a jog. DFT data points that the jog-punching operates spontaneously once the number of clusterized H atoms exceeds eight. This information coupled with the continuum rate theory model provides an adequate description of the depth profile typically observed after high flux plasma exposure in W. The density of supercritical hydrogen bubbles, predicted by the proposed model, was also confirmed by the TEM study. Hence, the proposed mechanism reconciles long-standing experimental observations of hydrogen isotopes retention and debates about its dependence on W microstructure. Moreover, this work provides an example of how the microstuctural features interfere non-equilibrium material properties becoming dominant in e.g. determination of susceptibility of W and its alloys to plasma exposure.

Additional information

Details on parametrization of DFTC and charge density maps explaining the origin of the 'hydrogen compensation' effect are provided as supplementary information and available online (stacks.iop.org/NF/54/042004/mmedia).

Competing financial interests

The authors declare no competing financial interests.

Acknowledgments

The work was supported by the European Fusion Programme. V. Dubinko acknowledges the support of the Erasmus Mundus Fusion EP fellowship.

References

[1] Kaufmann M. and Neu R. 2007 *Fusion Eng. Des.* **82** 521
[2] Zinkle S.J. 2005 *Phys. Plasmas* **12** 058101
[3] Ahlgren T., Heinola K., Vörtler K. and Keinonen J. 2012 *J. Nucl. Mater.* **427** 152
[4] Roszell J.P., Haasz A.A. and Davis J.W. 2011 *J. Nucl. Mater.* **415** S641
[5] Heinola K., Ahlgren T., Nordlund K. and Keinonen J. 2010 *Phys. Rev.* B **82** 094102
[6] 't Hoen M.H.J., Tyburska-Pûschel B., Ertl K., Mayer M., Rapp J., Kleyn A.W. and Zeijlmans van Emmichoven P.A. 2012 *Nucl. Fusion* **52** 023008
[7] Schmid K., Rieger V. and Manhard A. 2012 *J. Nucl. Mater.* **426** 247
[8] Zhou H.B., Liu Y.L., Jin S., Zhang Y., Luo G.N. and Lu G.H. 2010 *Nucl. Fusion* **50** 025016
[9] Ogorodnikova O.V., Roth J. and Mayer M. 2008 *J. Nucl. Mater.* **373** 254
[10] Haasz A.A., Poon M., Macaulay-Newcombe R.G. and Davis J.W. 2001 *J. Nucl. Mater.* **290–293** 85
[11] Johnson D.F. and Carter E.A. 2010 *J. Mater. Res.* **25** 315
[12] Zayachuk Y., 't Hoen M.H.J., van Emmichoven P.A.Z., Terentyev D., Uytdenhouwen I. van Oost G. 2013 *Nucl. Fusion* **53** 013013
[13] Kresse G. and Hafner J. 1993 *Phys. Rev.* B **47** 558
[14] Blochl P.E. 1994 *Phys. Rev.* B **50** 17593
[15] Perdew J., Wang Y. and Engel E. 1991 *Phys. Rev. Lett.* **66** 508
[16] Henkelman G. and Jonsson H. 2000 *J. Chem. Phys.* **113** 9978
[17] Cai W., Bulatov V.V., Chang J.P., Li J. and Yip S. 2003 *Phil. Mag.* **83** 539
[18] Ventelon L. and Willaime F. 2007 *J. Comput.-Aided Mater. Des.* **14** 85
[19] Li H., Wurster S., Motz C., Romaner L., Ambrosch-Draxl C. and Pippan R. 2012 *Acta Mater.* **60** 748
[20] Vitek V. 1974 *Cryst. Lattice Defects* **5** 1
[21] Heinola K. and Ahlgren T. 2010 *J. Appl. Phys.* **107** 113531
[22] Fu C.C. and Willaime F. 2007 *J. Nucl. Mater.* **367** 244
[23] Zayachuk Y., 't Hoen M.H.J., van Emmichoven P.A.Z., Uytdenhouwen I. and van Oost G. 2012 *Nucl. Fusion* **52** 103021
[24] Ryazanov A.I., Arutyunova G.A., Manichev V.M., Sokursky Y.N. and Chuev V.I. 1985 *J. Nucl. Mater.* **135** 232
[25] Dubinko V.I., Hu S., Li Y., Henager C.H. and Kurtz R.J. 2012 *Phil. Mag.* **92** 4113
[26] Frauenfelder R. 1968 *J. Vac. Sci. Technol.* **6** 388
[27] Zayachuk Y. 2013 Deuterium retention in tungsten and tungsten–tantalum alloys under high-flux plasma exposure *PhD Thesis* Faculty of Engineering, Ghent University (ISBN: 9789 0857 8635 1)